Additional file 1. Supplementary Methods, Supplementary Figures and Supplementary Tables

Supplementary Methods

Cell lines RRID and culture treatments

Research Resource Identifiers (RRIDs) of NSCLC cell lines are provided: A549 ATCC CCL-185, RRID:CVCL_0023; NCI-H1299 ATCC CRL-5803, RRID: CVCL_0060; NCI-H1650 CRL-5883, RRID:CVCL_1483; HCC-2935 CRL-2869, RRID:CVCL_1265; NCI-H2030 CRL-5914, RRID:CVCL_1517; NCI-H1975 CRL-5908, RRID:CVCL_1511.

Recombinant human IFNβ (#8499-IF-010, R&D Systems) was added to cell media at 50 ng/ml; anti-Interferon-α/β Receptor Chain 2 Antibody (Millipore Cat# MAB1155, RRID:AB_2122758) was added at 1µg/ml; JAK Inhibitor I (#420099, Merck) at 5 µM; human TGFβ1(#240-B-010/CF, R&D Systems) at 5 ng/ml.

The RIG-I agonist M8 (kindly provided by John Hiscott, Istituto Pasteur Italia-Cenci Bolognetti Foundation) (1) was delivered to cells using Lipofectamine®RNAiMAX Transfection Reagent (#13778075, Invitrogen) according to the manufacturer's protocol. Polyinosinic-polycytidylic acid (poly I:C) (#4287; TOCRIS) was delivered to cells using Lipofectamine™ 2000 Transfection Reagent (#116680191, Invitrogen) at 1µg/ml, according to the manufacturer's instructions.

Transfection and Small interfering RNA (siRNA)

A549 cells were infected with pMSCV/pMSCV11a vectors (2). Selection was carried out with 500 µg/ml of G418 (Invitrogen).

Transfection with siRNA was performed with Lipofectamine® RNAiMAX Transfection Reagent (#13778075, Invitrogen) according to the manufacturer's instructions. Cancer cells were transfected with: hMENA(t)-specific pooled siRNA duplexes (siGENOME SMART pool Human ENAH,

#FE5M021932020050), CDH1-specific pooled siRNA duplexes (siGENOME SMART pool Human CDH1, #M-003877-02), and ON-TARGET plus Non-targeting Control Pool (#FE5D0018101050), all from GE Healthcare, Dharmacon. DDX58-specific pooled of three siRNAs (DDX58 Silencer Pre-Designed siRNA, #134222) was from Ambion. Specific hMENA^{11a} silencing was performed as previously reported (3). Knockdown efficiency was assessed by Quantitative real-time RT–PCR (qRT-PCR) and the effects of silencing were evaluated at 48-72 h from the transfection.

RNA extraction and analysis

Total RNA (5 μg) was isolated from cells with Trizol reagent (Invitrogen) and reverse transcribed using first-strand cDNA synthesis kit (#27-9261-01, GE Healthcare) according to the manufacturer's protocol.

qRT–PCR was performed on an ABI Prism 7500 Real-time PCR instrument (Applied Biosystems). The reactions were carried out in triplicates. TaqMan Gene Expression Assays were used for the amplification and quantification of: STAT1 (Hs01013996_m1; Applied Biosystems), CXCL8 (Hs00174103_m1; Applied Biosystems), IL6 (Hs00174154_m1; Applied Biosystems), CXCL1(Hs00236937_m1; Applied Biosystems), CDH1(Hs01013953_m1; Applied Biosystems), CD274 (Hs01125301_m1; Applied Biosystems), DDX58 (Hs01861436_m1; Applied Biosystems), ISG15 (Hs00192713_m1; Applied Biosystems), MX1 (Hs00895608_m1; Applied Biosystems), OASL (Hs00984387_m1; Applied Biosystems), IFI44L (Hs00915292_m1; Applied Biosystems), ENAH (Hs00403109_m1; Applied Biosystems), IFNB1 (Hs.PT.58.39481063.g; Integrated DNA Technologies). qRT-PCR for hMENA^{11a} mRNA quantification was performed with custom designed probe and primers from Applied Biosystems (TaqMan MGB Probe: 5'-CTCCAGACGGGATTCT-3'; forward primer: 5'-ATGGCAGCAAGTCACCTGTTAT-3'; reverse primer: 5'-TGTAATGAATCATAGGACCTGTTGTCAAAA-3').

Human hypoxanthine phosphoribosyltransferase 1 gene (HPRT1) (Hs99999909_m1; Applied Biosystem) was used as an endogenous control. The comparative Ct method (2−ΔΔ/Ct method) was used to determine changes in relative levels of different genes (4).

RNA-Seq

Total RNA was extracted from NSCLC cell lines using Qiazol (Qiagen, IT), purified from DNA contamination through a DNase I (Qiagen, IT) digestion step and further enriched by Qiagen RNeasy columns. Integrity of the RNA was assessed by Agilent 2100 Bioanalyzer (Agilent Technologies, CA). RNA libraries for sequencing were generated in triplicate using 500 ng of RNA for each sample according to the Illumina TruSeq Stranded Total RNA kit with an initial ribosomal depletion step using Ribo Zero Gold (Illumina, CA). The libraries were sequenced in paired-end mode (2x75 bp) with NextSeq 500 (Illumina, CA).

Assay for transposase-accessible chromatin using sequencing (ATAC-seq)

To investigate chromatin accessibility dynamics, the ATAC-seq protocol developed by Buenrostro et al. was used, with minor modifications (5).

Luciferase Reporter Assay

Cells were seeded in 24-well plates, transfected with indicated siRNAs and 24 hours later, transfected with specific inducible reporter constructs (NF-kB #CCS-013L or IRF-1 #CCS-7040L Cignal Reporter Assay Kits, QIAGEN) using Lipofectamine ™ 2000 Transfection Reagent (#116680191, Invitrogen). Luciferase assays were developed 48 hours later with Dual-Glo Luciferase Assay System (Promega), following the manufacturer's protocol. The luminescence was detected using the GloMax96 Microplate Luminometer (Promega, WI). Firefly luciferase activities were normalized to Renilla luciferase activities.

Western Blot analysis

Protein extraction and Western blot analyses were carried out as previously described (6). Nuclear and cytoplasmic fractions were prepared using NE-PER Nuclear Cytoplasmic Extraction Reagents kit (#78835, Pierce). Protein concentrations were determined by bicinchoninic acid (BCA) assay (#23225, Pierce) according to the manufacturer's instructions. The following antibodies were used: hMENA^{11a} Mouse antibody (6) and anti-Pan hMENA (6); from Cell Signalling Technology: anti-phospho-STAT-1 (Tyr701) Rabbit antibody (#9167, RRID:AB_561284; 1:1000), anti-STAT-1 Rabbit antibody (#14994, RRID:AB_2737027; 1:1000), anti-PD-L1 XP® Rabbit antibody (#13684, RRID:AB_2687655; 1:1000), anti-IRF-1 Rabbit antibody (#8478, RRID:AB_10949108; 1:1000), anti-phospho-IRF-3 (Ser396) Rabbit antibody (#4947, RRID:AB_823547; 1:1000), anti-IRF-3 Rabbit antibody (#4302, RRID:AB_1904036; 1:1000), anti-STING Rabbit antibody (#13647, RRID:AB_2732796; 1:1000), anti-phospho-STING (Ser366) Rabbit antibody (#19781, RRID:AB_2737062; 1:1000), anti-RIG-I Rabbit antibody (#3743, AB_2269233; 1:1000), anti-Lamin A/C Mouse antibody(#4777, RRID:AB_10545756; 1:2000), anti-α-Tubulin Rabbit antibody (#2125, RRID:AB_2619646; 1:1000); from BD Transduction Laboratories: anti-E-cadherin Mouse antibody (#610182, RRID:AB_397581; 1:2000); from Sigma-Aldrich: anti-β-actin Mouse antibody (#A4700, RRID:AB_476730; 1:2500); from Santa Cruz Biotechnology anti-HSP70 Mouse antibody (#sc-24, RRID:AB_627760; 1:2000). Secondary antibodies used were from Bio-Rad: goat anti-Rabbit HRP (#170-6515, RRID:AB_11125142; 1:2000) and goat anti-Mouse HRP (#170-6516, RRID:AB_11125547; 1:2000).

Harvesting tumor-conditioned media

To obtain culture supernatants for the generation of tumor-conditioned media (CM), approximately 2×10^5 cancer cells/well were plated in six-well plates and grown to 80% confluence. Cells were grown in serum-free media for 24 h. CMs were harvested, centrifuged to remove non-adherent cells and debris.

Cytokine analysis

Levels of IFNβ (PBL, #41415-1) and of IL6 (#D6050), IL8 (#D8000C), CXCL1(#DGR00B) (all from R&D Systems) were determined by ELISA assays according to the manufacturer's protocol.

Levels of 40 different chemokines and cytokines were evaluated by Pro Human Cytokine 40-Plex Assays panel (Bio-Rad, Hercules, CA, USA), according to the manufacturer's instructions. Cytokines were quantified on the Luminex platform using the Bio-Plex MagPix instrument (Bio-Rad, Hercules, CA, USA) and the Bio-Plex Manager MP software was used for data acquisition and analysis. All the samples were run in duplicate and ten-point standard curve, positive, negative sample were run for each cytokine. Determinations that were designated "Out of Range Below" (i.e. below the limit of quantification) by the analytical software were arbitrarily filled with a zero value.

Immunofluorescence

Cells (3×10^5) were cultured on glass coverslips pre-coated with 0,2 % gelatine and grown for 48 h before fixing and permeabilizing as previously reported (6). Cells were stained with: anti- IRF-1 Mouse antibody (sc-137061, RRID:AB_2126721; 1:100), anti-IRF-2 Mouse antibody (sc-101069, RRID:AB_1124709; 1:250) from Santa Cruz Biotechnology; anti-E-Cadherin Mouse antibody (#610182, RRID:AB_397581; 1:200) and anti-ZO-1 Mouse antibody (#610967, RRID:AB_398280; 1:250) from BD Transduction Laboratories; anti-Vimentin Rabbit antibody (#5741, RRID:AB_10695459; 1:100; Cell Signalling Technology). Secondary antibodies used were Alexa Fluor 488-conjugated donkey anti-mouse (#A11017, RRID:AB_143160; 1:250) or Alexa Fluor 594-conjugated donkey anti-rabbit antibodies (#A1107, RRID:AB_1420572; 1:250). Actin filaments were stained with Alexa Fluor™ 594 Phalloidin (1:250) all from Thermo Fisher Scientific. The glass coverslips were mounted with the VECTASHIELD® MOUNTING MEDIUM with DAPI (4'6-diamidino-2-phenylindole) (Vector Laboratories).

Fluorescence signals were captured by using a Leica DMIRE2 microscope equipped with a Leica DFC 350FX camera and elaborated by Leica FW4000 deconvolution software (Leica, Solms, Germany) or Zeiss LSM 880 with Airy scan confocal laser scanning microscope equipped with a

20× air or 63X/1.23 NA oil immersion objectives. Lasers 488 and 594 nm were used to excite the fluorophores. The Zeiss Zen control software (Zeiss, Germany) was used for image analysis

Senescence-Associated β-Galactosidase (SA-β-gal) Assay

Cells were fixed in 2% paraformaldehyde for 15 min and treated at 37 °C with SA-β-Gal solution: 1 mg/ml of 5-bromo-4-chloro-3-indolyl P3-D-galactoside (X-Gal), 40 mM citric acid/sodium phosphate (pH 6.0), 5 mM potassium ferrocyanide, 5 mM potassium ferricyanide, 150 mM NaCl, 2 mM MgCl2. Blue-stained senescent cells images were captured by a light microscopy (Leica DM IL LED).

Flow cytometry

Surface-staining of cancer cell lines was performed for 30 min at 4°C using PE-CD274 mAb (#557924 BD Biosciences, RRID:AB_647198). Surface-staining of macrophages was performed for 30 min at 4°C using various combinations of the following mAbs, all from BD Biosciences: BV786-CD16 (#563690, RRID:AB_2744299), BV421-CD206 (#564062, RRID:AB_2738570), BB515-CD80 (#565008, RRID:AB_2744452), BV480-CD86 (#566131, RRID:AB_2739530), BV605-CD11b (#562721, RRID:AB_2737745), PE-CD274 (#557924, RRID:AB_647198), APC-CD273 (#557926, RRID:AB_647162), BV510-HLA-DR (#563083, RRID:AB_2737994), perCP-Cy5.5-CD163 (#563887, RRID:AB_2738467) and PE-VISTA (#566669, RRID:AB_2739762). Human Fc Block™ (#564220, BD Biosciences) was used according to manufacturer's instructions to stain macrophages before adding mAbs. Intracellular staining was performed by Intrasure kit (#641778, BD Bioscience) according to manufacturer's instructions, combining surface mAbs with the following intracellular mAbs from BD Bioscience: APC-IL10 (#554707, RRID:AB_398582) and Alexafluor488-TGFβ (#562545, RRID:AB_2737645). Dead cells were excluded by propidium iodide staining (#195458, MP Biomedicals) or BD Horizon™ Fixable Viability Stain 780 (FVS780) (#565388, BD Biosciences), according to manufacturer's instructions. Cells were acquired on BD

FACSCanto II and BD FACS Celesta ™ flow cytometers (BD Biosciences) and analyzed using BD FACS DIVA™ and Flowjo software (BD Biosciences).

Computational methods

RNA-seq analysis

RNA-sequencing data were independently analysed by following the *Kallisto* (v.0.46.0) and *Sleuth* (v.0.30.0) pipeline. Sequencing quality of each sample was assessed with *FASTQC* (v0.11.91) and summarized with *MultiQC* (v.1.9). Read quantification was performed with the function "quant" of the *Kallisto* tool (parameters: -b 100). The pseudoalignment was performed against the reference genome GRCh37 downloaded from NCBI and subsequently indexed with the function "index" of the *Kallisto* tool. Reads counts were normalized with the function "sleuth prep" and used to perform a differential analysis with the function "sleuth fit" fitting a full model. Principal component analysis (PCA) was executed pre- and post-normalization. Pre-normalized PCA was executed using the function "prcomp" of the *stats* (v.4.0.220) R package and plotted through the function "autoplot" of the *ggfortify* (v.0.4.11) R package. Post-normalized PCA was carried out with the function "plotpca" of the *Sleuth* package in R. Wald test was performed with the function "sleuth_wt" and only those significant gene (q-value<0.05) were maintained. The beta-value obtained from the test was used to discriminate between UP (b>1) and DOWN (b<-1) regulated genes. A volcano plot showing the statistical significance (q-value) by the magnitude of change [log2(b)] of each gene was created with the *ggplot2* R package.

ATAC-seq analysis

ATAC-seq peak calling: ATAC profiles were aligned to the reference genome hg19. Reads were quality controlled with FastQC v0.11.5 and aligned to the reference genome using bowtie 2.3.4.2 (5) with default parameters. The generated sequence alignments were converted into binary files (BAM), then sorted and indexed using the SAMtools V1.7 (7). ATAC-seq peaks were generated

using MACS v2.2.5 (8) with parameters '--nomodel --shift -100 --extsize 200 -B --SPMR --call-summits -q 0.01'. Peaks in bedGraph format (.bdg) were converted in bigWig (.bw) format using bedGraphToBigWig tool. All peaks matching blacklisted regions were discarded from further processing. IGV (9) was used to visualize peak signals.

Global ATAC sequencing profiles: ATAC-seq global profiles of each experiment were obtained by building a master list of accessible sites for each experimental group by pooling the significant peaks in the control and treatment group with an in-house pipeline based on BEDTOOLS v2.25.0 (10) and custom BASH scripts. The master list of ATAC-seq sample groups was produced with a multistep procedure: I-To identify the common overlapping signal amongst all the samples, peaks were intersected using BEDTOOLS multiinter. II-The book-ended regions from the core signal file were merged using BEDTOOLS merge, then intersected with the original peak calls and sorted. Each master list represented the reference table used as input to ComputeMatrix v 3.1.3 tool available in the DeepTools suite (11). Relative BigWig files of each group were then used to populate the final matrix enrichment, which then was used as input to plot the global profiles with PlotProfile v3.1.3 available in DeepTools.

ATAC-seq sequencing differential analysis: Differential analysis of ATAC-seq data was obtained using an in-house workflow, which deploys the edgeR suite. After building the master list of each experimental group pooling control and treatment as described above, we assigned the raw counts from to each relative locus using bedtoolsmulticov v2.29.2. Raw counts were previously deprived of duplicates utilising MarkDuplicates tool available in GATK suite v4.1.4.1(12).Counts were processed and normalized with the TMM method. The differential analysis was performed using an in-house script which relies on the edgeR "exactTest" function. Data were adjusted for Benjamini Hochberg correction. The sites showing both FDR<0.05 and log2(fold change) > |1.2| were considered significant.

Nanostring transcriptome data analysis

Raw counts were used to perform a Differential Gene Expression Analysis (DGEA) between PRs and GRs applying a likelihood-ratio test (generalized linear model) with the R package NanostringDiff (13). Genes with logFC(Fold Change) ≥ 0.5 or ≤ -0.5 and q-value≤0.1 were considered modulated and were taken into consideration for downstream analyses. Raw counts were normalized using the geNorm method (14) using normalization factors computed from positive and negative control probes and housekeeping genes included in the panel. For each patient, scores for an IFN gene signature (provided by NanoString), an IFN module signature (15), a Macrophage gene signature (provided by NanoString, based on CD84, CD68, CD163 and MS4A4A genes) and an IFN-related Macrophage gene signature (16) were calculated by averaging the expression values of the genes in each signature. The distributions of the signature scores were compared using a two-tailed Student's t test.

PD-L1 score (Supplementary Table 2) was evaluated by grouping the normalized counts from the Nanostring profiling into 3 expression level groups based on the ranking of CD274 expression levels. All plots and statistical analyses were performed in the R environment v4.0.1 [*R Core Team (2021). R: A language and environment for statistical computing. R Foundation for Statistical Computing, Vienna, Austria. URL https://www.R-project.org/.*] using in-house scripts.

Clinical validation in advanced NSCLC from the POPLAR and OAK trials

To demonstrate that ESRP1 and ENAH gene expressions could serve as a proxy for hMENA^{11a} splicing variant levels, we investigated the association between the expression levels of ESRP1 and ENAH and the expression levels of hMENA^{11a} (ENST00000366844.7) in the 1.011 samples of the Lung Cancer cohort from The Cancer Genome Atlas database (17).

Firstly, samples were stratified based on hMENA^{11a} transcript expression using the tertiles as thresholds and considering as “HIGH” the patients with expression levels in the third tertile (above the 66th percentile) and “LOW” the patients with expression levels in the first tertile (below the 33rd percentile). Then, considering that ESRP1 regulates the inclusion of 11a exon (18), samples were

stratified based on ENAH and ESRP1 genes expression levels using tertiles as thresholds and considering "HIGH" the patients with both expression levels of ESRP1 above the 33rd percentile and expression levels of ENAH above the 66th percentile. Conversely, patients with both expression levels of ESRP1 below the 33rd percentile and expression levels of ENAH below the 66th percentile were considered as "LOW". Thus, a confusion matrix was built to assess the accuracy, precision, and recall of the prediction. To ensure the robustness of our stratification model, we performed 1000 iterations of the same analysis for each randomly sampled subset consisting of 100, 250, 500, and 750 patients (Figure S6). Results showed an average precision, accuracy and recall scores of 0.95, 0.87 and 0.83 respectively, suggesting that the combined expressions of ENAH and ESRP1 genes could be used as a surrogate of hMENA^{11a} splicing variant level, thereafter named ENAH-11a.

OAK and POPLAR datasets were obtained from the European Genome-Phenome Archive (EGA) after formal request. Patients who underwent ICB therapy were stratified based on ENAH-11a expression (as above described) and Best Confirmed Overall Response (BCOR) classes, considering Partial Response (PR), Complete Response (CR) or Stable Disease (SD) as "Good Response" (GR), and Progressive Disease (PD) as "Poor Response" (PR).

The IFN and Macrophage signature genes [provided by NanoString and by Barkley and Ma (15, 16) were log2-scaled, and the average values were used as scores for the respective gene signatures. GR samples showing high expression of ENAH-11a, and PR samples showing low expression of ENAH-11a, were selected and compared, using two-tailed Student's T test to assess significantly different distributions. The CD8 T cell exhaustion signature genes from (19) were log2-scaled and the average values were used as score. GR and PR samples were compared using two-tailed Student's T test to assess significantly different distributions.

Cell type deconvolution

Cell type deconvolution of the Nanostring internal cohort was derived from the Nanostring nCounter® Advanced Analysis Software, using default parameters.

Cell type deconvolution of PR/GR patients from the OAK and POPLAR studies stratified as above was performed with two different computational tools: CibersortX (20) and MCP-counter (21). In details, for CibersortX absolute mode, batch correction and 1000 permutations were used as parameters. Three relevant immune cell classes were obtained aggregating cells corresponding to distinct immune cell types as follows: Macrophages: “Macrophages M0”, “Macrophages M1” and “Macrophages M2”; Dendritic cells (DCs): “Dendritic cells activated” and “Dendritic cells resting”; CD8 T cells: “CD8 T cells”. For MCP-counter default parameters for RNA-Seq data were used and “Monocytic lineage”, “Myeloid Dendritic cell” and “CD8 T cell” abundances were selected for the analysis. For each immune cell class the abundance score was plotted comparing GR and PR samples using two-tailed Student’s T test to assess significantly different distributions.

Additional references

1. Castiello L, Zevini A, Vulpis E, Muscolini M, Ferrari M, Palermo E, et al. An optimized retinoic acid-inducible gene I agonist M8 induces immunogenic cell death markers in human cancer cells and dendritic cell activation. Cancer Immunol Immunother. 2019;68(9):1479-92.

2. Di Modugno F, Spada S, Palermo B, Visca P, Iapicca P, Di Carlo A, et al. hMENA isoforms impact NSCLC patient outcome through fibronectin/β1 integrin axis. Oncogene. 2018;37(42):5605-17.

3. Trono P, Di Modugno F, Circo R, Spada S, Di Benedetto A, Melchionna R, et al. hMENA(11a) contributes to HER3-mediated resistance to PI3K inhibitors in HER2-overexpressing breast cancer cells. Oncogene. 2016;35(7):887-96.

4. Livak KJ, Schmittgen TD. Analysis of relative gene expression data using real-time quantitative PCR and the 2(-Delta Delta C(T)) Method. Methods. 2001;25(4):402-8.

5. Buenrostro JD, Wu B, Chang HY, Greenleaf WJ. ATAC-seq: A Method for Assaying Chromatin Accessibility Genome-Wide. Curr Protoc Mol Biol. 2015;109:21.9.1-.9.9.

6. Di Modugno F, Iapicca P, Boudreau A, Mottolese M, Terrenato I, Perracchio L, et al. Splicing program of human MENA produces a previously undescribed isoform associated with invasive, mesenchymal-like breast tumors. Proc Natl Acad Sci U S A. 2012;109(47):19280-5.

7. Langmead B, Salzberg SL. Fast gapped-read alignment with Bowtie 2. Nat Methods. 2012;9(4):357-9.

8. Li H, Handsaker B, Wysoker A, Fennell T, Ruan J, Homer N, et al. The Sequence Alignment/Map format and SAMtools. Bioinformatics. 2009;25(16):2078-9.

9. Zhang Y, Liu T, Meyer CA, Eeckhoute J, Johnson DS, Bernstein BE, et al. Model-based analysis of ChIP-Seq (MACS). Genome Biol. 2008;9(9):R137.

10. Robinson JT, Thorvaldsdóttir H, Winckler W, Guttman M, Lander ES, Getz G, et al. Integrative genomics viewer. Nat Biotechnol. 292011. p. 24-6.

11. Quinlan AR, Hall IM. BEDTools: a flexible suite of utilities for comparing genomic features. Bioinformatics. 2010;26(6):841-2.

12. Ramírez F, Dündar F, Diehl S, Grüning BA, Manke T. deepTools: a flexible platform for exploring deep-sequencing data. Nucleic Acids Res. 2014;42(Web Server issue):W187-91.

13. Wang H, Horbinski C, Wu H, Liu Y, Sheng S, Liu J, et al. NanoStringDiff: a novel statistical method for differential expression analysis based on NanoString nCounter data. Nucleic Acids Res. 2016;44(20):e151.

14. Vandesompele J, De Preter K, Pattyn F, Poppe B, Van Roy N, De Paepe A, et al. Accurate normalization of real-time quantitative RT-PCR data by geometric averaging of multiple internal control genes. Genome Biol. 2002;3(7):Research0034.

15. Barkley D, Moncada R, Pour M, Liberman DA, Dryg I, Werba G, et al. Cancer cell states recur across tumor types and form specific interactions with the tumor microenvironment. Nat Genet. 2022;54(8):1192-201.

16. Ma RY, Black A, Qian BZ. Macrophage diversity in cancer revisited in the era of single-cell omics. Trends Immunol. 2022;43(7):546-63.

17. Vivian J, Rao AA, Nothaft FA, Ketchum C, Armstrong J, Novak A, et al. Toil enables reproducible, open source, big biomedical data analyses. Nat Biotechnol. 35. United States2017. p. 314-6.

18. Warzecha CC, Jiang P, Amirikian K, Dittmar KA, Lu H, Shen S, et al. An ESRP-regulated splicing programme is abrogated during the epithelial-mesenchymal transition. Embo j. 2010;29(19):3286-300.

19. Chu Y, Dai E, Li Y, Han G, Pei G, Ingram DR, et al. Pan-cancer T cell atlas links a cellular stress response state to immunotherapy resistance. Nat Med. 2023;29(6):1550-62.

20. Newman AM, Steen CB, Liu CL, Gentles AJ, Chaudhuri AA, Scherer F, et al. Determining cell type abundance and expression from bulk tissues with digital cytometry. Nat Biotechnol. 2019;37(7):773-82.

21. Becht E, Giraldo NA, Lacroix L, Buttard B, Elarouci N, Petitprez F, et al. Estimating the population abundance of tissue-infiltrating immune and stromal cell populations using gene expression. Genome Biol. 2016;17(1):218.

Supplementary Figures

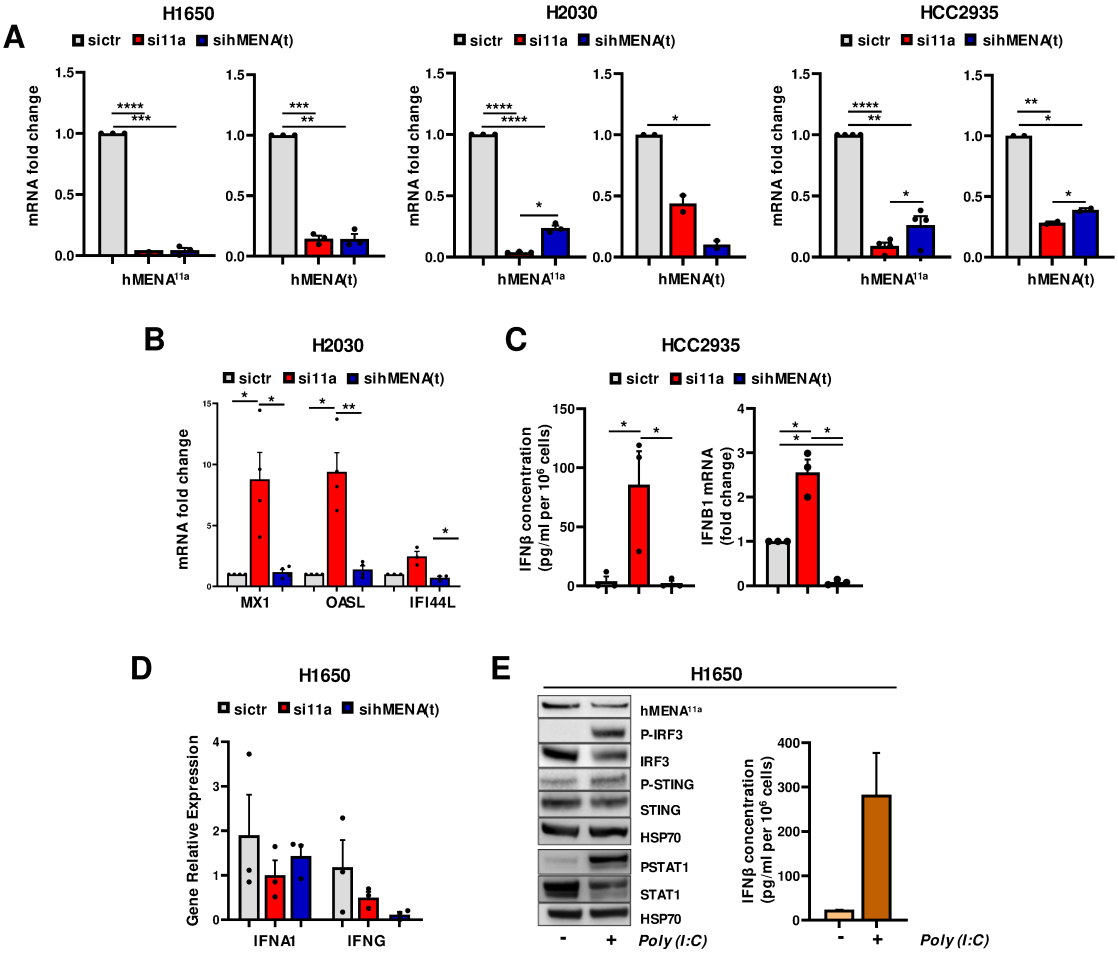
A
H1650
H2030
HCC2935
sictr
si11a
sihMENA(t)
mRNA fold change
hMENA11a
hMENA(t)
B
H2030
MX1
OASL
IFI44L
C
HCC2935
IFNβ concentration (pg/ml per 10^6 cells)
IFNB1 mRNA (fold change)
D
H1650
Gene Relative Expression
IFNA1
IFNG
E
H1650
hMENA11a
P-IRF3
IRF3
P-STING
STING
HSP70
PSTAT1
STAT1
HSP70
Poly (I:C)

Figure S1.

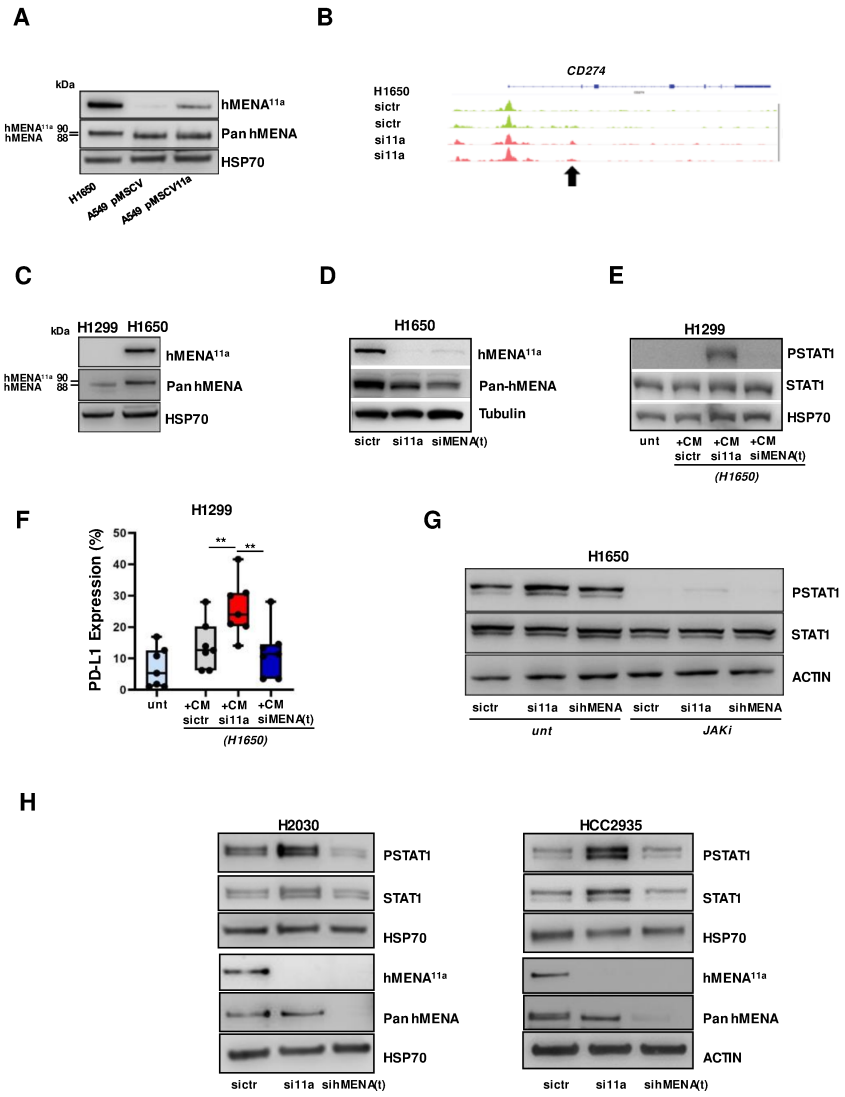
A
kDa
hMENA11a
hMENA
90
88
hMENA11a
Pan hMENA
HSP70
H1650
A549 pMSCV
A549 pMSCV11a
B
CD274
H1650
sictr
sictr
si11a
si11a
C
kDa
H1299
H1650
hMENA11a
hMENA11a
hMENA
90
88
Pan hMENA
HSP70
D
H1650
hMENA11a
Pan-hMENA
Tubulin
sictr
si11a
siMENA(t)
E
H1299
PSTAT1
STAT1
HSP70
unt
+CM sictr
+CM si11a
+CM siMENA(t)
(H1650)
F
H1299
PD-L1 Expression (%)
50
40
30
20
10
0
**
**
unt
+CM sictr
+CM si11a
+CM siMENA(t)
(H1650)
G
H1650
PSTAT1
STAT1
ACTIN
sictr
si11a
sihMENA
sictr
si11a
sihMENA
unt
JAKi
H
H2030
PSTAT1
STAT1
HSP70
hMENA11a
Pan hMENA
HSP70
sictr
si11a
sihMENA(t)
HCC2935
PSTAT1
STAT1
HSP70
hMENA11a
Pan hMENA
ACTIN
sictr
si11a
sihMENA(t)

Figure S2.

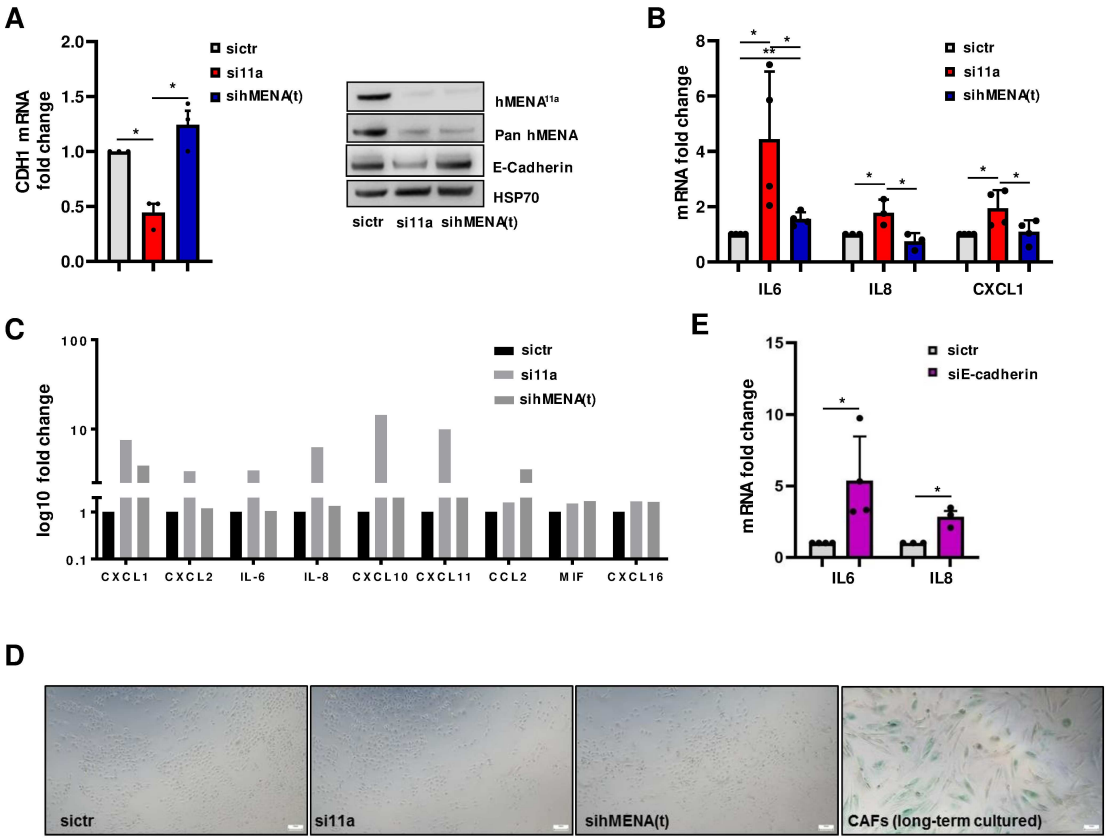
A
CDH1 mRNA fold change
sictr
si11a
sihMENA(t)
hMENA11a
Pan hMENA
E-Cadherin
HSP70
sictr si11a sihMENA(t)
B
mRNA fold change
IL6
IL8
CXCL1
C
log10 fold change
CXCL1 CXCL2 IL-6 IL-8 CXCL10 CXCL11 CCL2 MIF CXCL16
E
siE-cadherin
D
sictr
si11a
sihMENA(t)
CAFs (long-term cultured)

Figure S3.

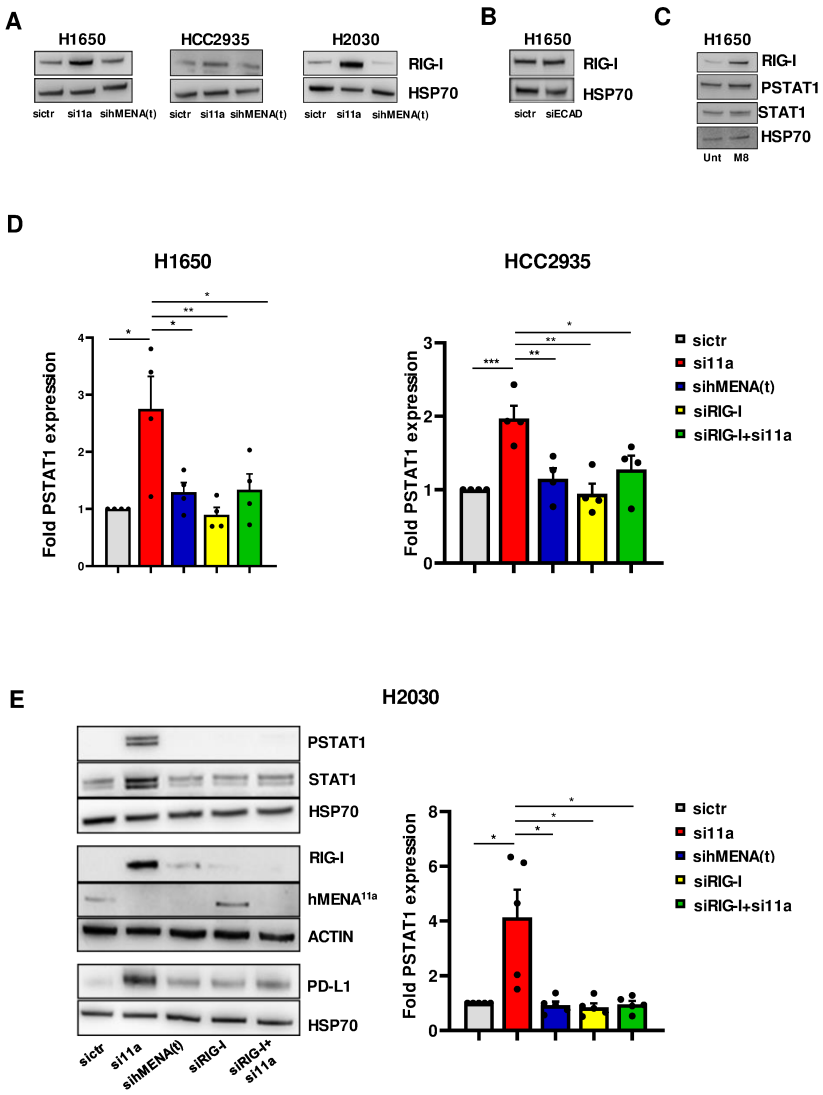
A
H1650
HCC2935
H2030
RIG-I
HSP70
sictr si11a sihMENA(t)
sictr si11a sihMENA(t)
sictr si11a sihMENA(t)
B
H1650
RIG-I
HSP70
sictr siECAD
C
H1650
RIG-I
PSTAT1
STAT1
HSP70
Unt M8
D
H1650
HCC2935
Fold PSTAT1 expression
sictr
si11a
sihMENA(t)
siRIG-I
siRIG-I+si11a
E
H2030
PSTAT1
STAT1
HSP70
RIG-I
hMENA11a
ACTIN
PD-L1
HSP70
sictr
si11a
sihMENA(t)
siRIG-I
siRIG-I+ si11a

Figure S4.

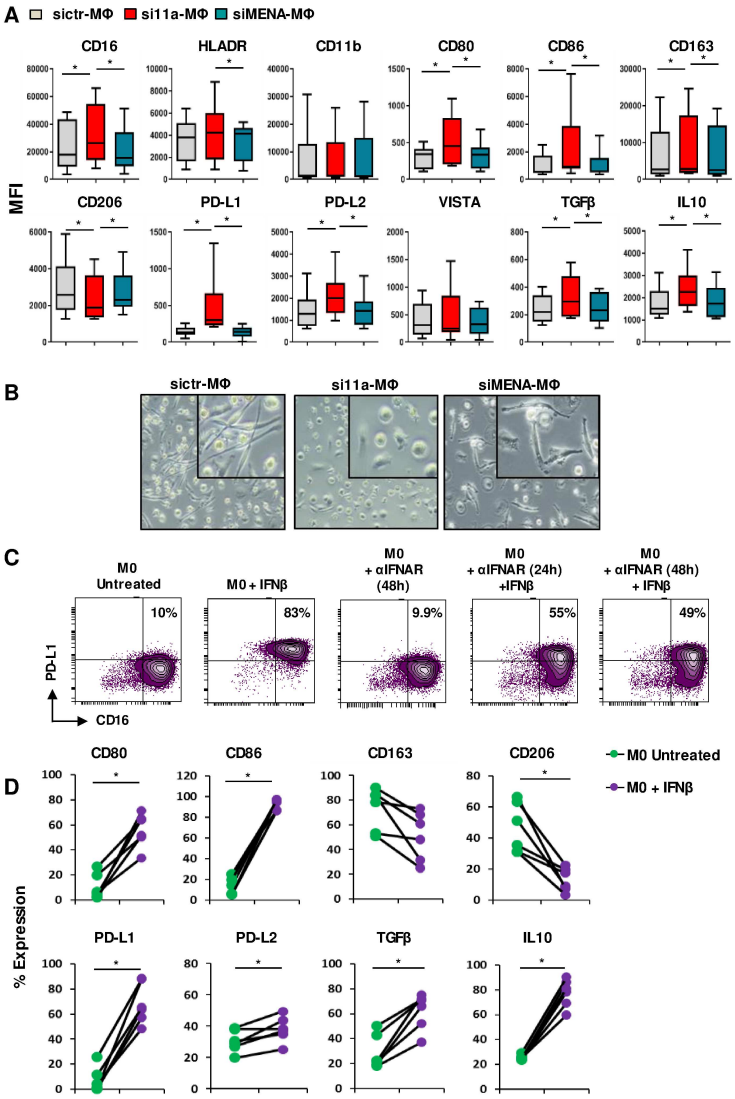
A
sictr-MΦ
si11a-MΦ
siMENA-MΦ
CD16
HLADR
CD11b
CD80
CD86
CD163
MFI
CD206
PD-L1
PD-L2
VISTA
TGFβ
IL10
B
sictr-MΦ
si11a-MΦ
siMENA-MΦ
C
M0 Untreated
M0 + IFNβ
M0 + αIFNAR (48h)
M0 + αIFNAR (24h) +IFNβ
M0 + αIFNAR (48h) + IFNβ
10%
83%
9.9%
55%
49%
PD-L1
CD16
D
CD80
CD86
CD163
CD206
M0 Untreated
M0 + IFNβ
% Expression
PD-L1
PD-L2
TGFβ
IL10

Figure S5.

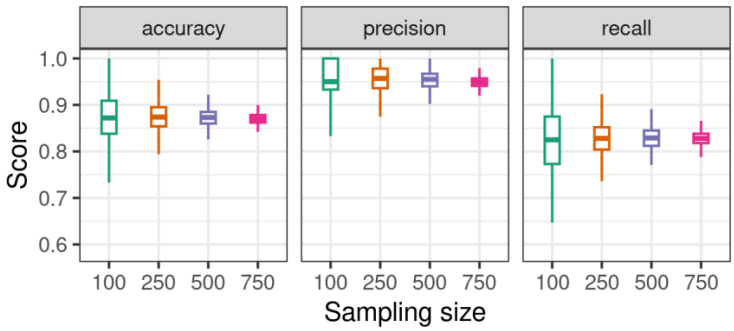
accuracy
precision
recall
Score
1.0
0.9
0.8
0.7
0.6
100 250 500 750
100 250 500 750
100 250 500 750
Sampling size

Figure S6.

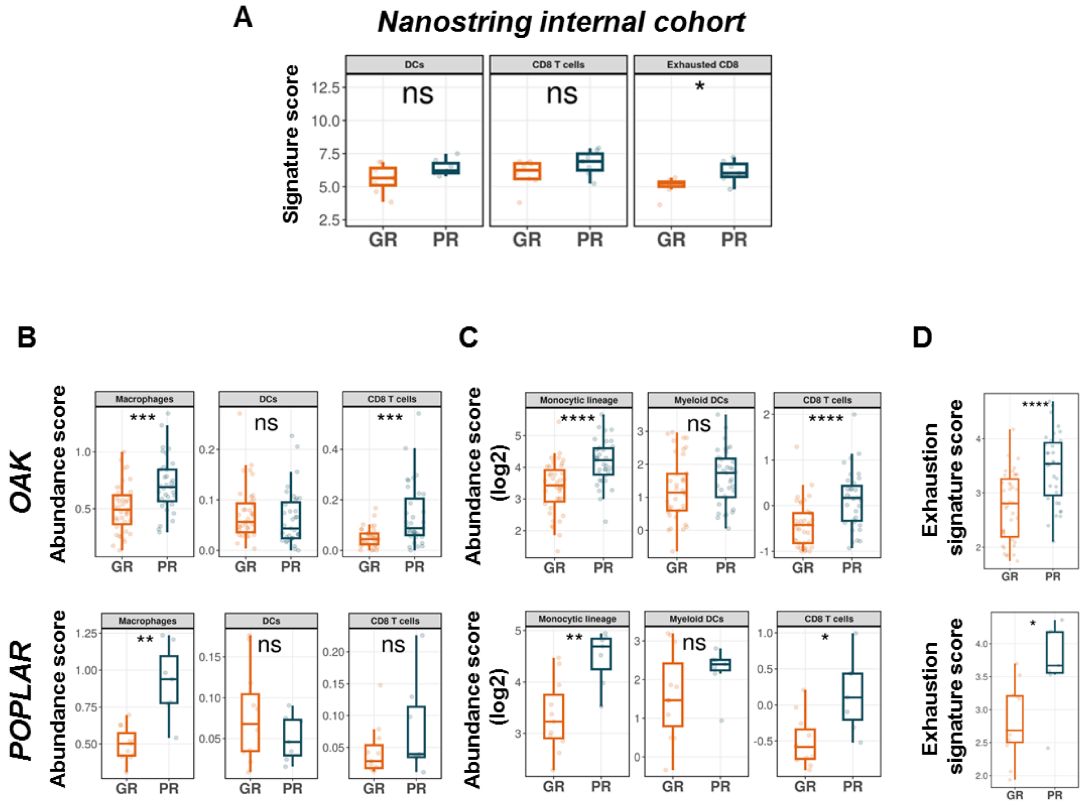

Figure S7

Figure legends

Figure S1. A qPCR results of mRNA levels of hMENA^{11a} and hMENA(t) in H1650, H2030 and HCC2935 sictr, si11a and sihMENA(t) cells. **B** qPCR results of mRNA levels of selected genes in sictr, si11a and sihMENA(t) H2030 cells. **C** Levels of IFNβ in supernatants evaluated by ELISA (***left***) and of IFNB1 mRNA by qRT-PCR (***right***) expressed as fold-change relative to control in HCC2935 sictr, si11a, sihMENA(t) cells. **D** qPCR results of mRNA levels of IFNα and IFNγ in H1650 cells treated as in (**A**). **E** ***Left panel***: Western blotting of H1650 cells, untreated or treated with polyinosinic acid-polycytidylic acid Poly(I:C), 100 ug/ml for four hours. ***Right panel***: levels of IFNβ analyzed by ELISA assay in supernatants of H1650 cells untreated or treated with Poly(I:C), 100 ug/ml for 24 hours. **A, B, C, D**: P values were calculated by two-tailed Student's t test.

Figure S2. hMENA^{11a} affects PD-L1 expression in NSCLC cell lines. **A** hMENA isoform expression levels analyzed by western blotting in H1650 and A549 pMSCV or pMSCV11a. **B** ATAC-Seq analysis of sictr and si11a H1650 cells indicates an open chromatin region (arrow) in the *CD274* locus in si11a cells. **C** hMENA isoform expression levels in H1299 and H1650 NSCLC cell lines analyzed by western blotting with specific antibodies. **D** hMENA isoform expression levels

analyzed by western blotting in sictr, si11a and sihMENA(t) H1650 cells, whose conditioned medium (CM) was used to treat H1299 cells as shown in (**E**). **E** STAT1 phosphorylation analyzed by western blotting in H1299 NSCLC cell line, untreated or treated for 24 hours with CM derived from sictr, si11a and sihMENA(t) H1650 cells. **F** PD-L1 expression in H1299 cells untreated or treated as in (**E**) analyzed by flow cytometry analysis. **G** Western blotting of sictr, si11a and sihMENA(t) H1650 cells, untreated (A) or treated with JAK inhibitor (5 μM) for 72 hours (B). **H** Western blotting of sictr, si11a and sihMENA(t) in H2030 and HCC2935 cells. **F**: P values were calculated by two-tailed Student's t test.

Figure S3. A E-cadherin expression at mRNA (***left***) and protein (***right***) levels analyzed in sictr, si11a and sihMENA(t) H1650 cells by qRT-PCR and western blot, respectively. **B** qPCR results of mRNA levels of the indicated genes evaluated in H1650 cells, treated as in (**A**)**. C** Levels of the indicated chemokines and cytokines in supernatants of sictr, si11a and sihMENA(t) H1650 cells quantified by Pro Human Cytokine 40-Plex Assays panel. **D** Senescence-Associated β-Galactosidase (SA-β-gal) Assay: βgal staining of H1650, treated as in (**A**)**.** Long-term cultured CAFs were used as an experimental control. **E** qRT-PCR results of mRNA levels of the indicated genes in sictr and siE-Cadherin H1650 cells. **A, B, E**: P values were calculated by two-tailed Student's t test.

Figure S4. A Western blotting analysis of sictr, si11a and sihMENA(t) H1650, HCC2935, H2030 cells. Anti-HSP70 was used as loading control. **B** Western blotting analysis of sictr and siE-cadherin (siE-cad) H1650 cells. **C** Western blotting analysis of H1650 cells untreated or treated with M8 (1μg/ml). **D** Levels of PSTAT1 in H1650 (**left**) and HCC2935 (***right***) cells were quantified by densitometry analysis using ImageJ and normalized to their respective actin or HSP70 levels and then expressed as fold change versus sictr. **E** (***left***) Western blotting analysis of sictr, si11a, sihMENA(t) siRIG-I (transfected with specific RIG-I siRNA) and siRIG-I+si11a H2030 cells. Anti-HSP70 was used as loading control. Representative blots of three independent experiments are reported. (***right***) Levels of PSTAT1in H2030 cells were quantified by densitometry analysis using ImageJ and normalized to their respective HSP70 and then expressed as fold change versus sictr.

Figure S5. A Analysis by flow cytometry of expression levels of macrophage markers in sictr-MΦs, si11a-MΦs, siMENA-MΦs, in terms of MFI (N = 9). **B** Representative phase contrast images showing morphological differences of sictr-MΦs, si11a-MΦs, siMENA-MΦs respectively. **C** Representative dot-plots of the expression level of PD-L1 *vs* CD16 in MΦs treated for 24 or 48 hours with anti-IFNAR (1μg/ml) and untreated or treated with IFNβ (50ng/ml) for 24 hours. Percentages of PD-L1+CD16+ cells are indicated. **D** Analysis by flow cytometry of selected macrophage marker expression levels in M0-MΦ stimulated for 24 hours with recombinant IFNβ (N = 6). Statistical significance was determined using Wilcoxon rank test, with Bonferroni correction for multiple comparison. * $P \leq 0.05$

Figure S6. Boxplots showing accuracy, precision and recall scores for the 1000 iterations of the randomly sampled subset comprising 100, 250, 500, and 750 patients. Accuracy= (TruePositives + TrueNegatives)/(Positives + Negatives); Precision = TruePositives / (TruePositives + FalsePositives); Recall= TruePositives / (TruePositives + FalseNegatives). Shown in the boxplots are the medians (horizontal lines), 25th to 75th percentiles (box outlines), and highest and lowest values within 1.5 times the interquartile range (vertical lines).

Figure S7. A Boxplots showing signature score distributions of three relevant immune cell type populations as calculated by Nanostring nCounter® Advanced Analysis Software suite in 8 good responder (GR) and 7 poor responder (PR) patients. **B-C.** Boxplots showing abundance score distributions of three relevant immune cell type populations obtained from CibersortX (**B**) and MCP-Counter (**C**) in OAK (upper panels) and POPLAR (lower panels) patients stratified as in Figure 6. **D** Boxplots showing the average of the exhaustion gene signature from (19), in OAK (upper panel) and POPLAR (lower panel) patients stratified as in Figure 6. **A-D**. Median and 1.5 IQR were plotted along with distribution comparison significance. *P* values were calculated using Student's test. * $P \leq 0.05$, ** $P \leq 0.01$, *** $P \leq 0.001$, *** $P \leq 0.0001$. ns, not significant.

Supplementary Table 1. **Mutational status of NSCLC cell lines**

Gene \ Cell lines	NCI-H1650	HCC2935	NCI-H2030	NCI-H1975	A549	NCI-H1299
ALK	wt	CNA	CNA	CNA	CNA	wt
EGFR	E746-A750del	E746-T751del; S752I	wt	L858R, T790M; CNA	wt	wt
KRAS	wt	wt	G12C	CNA	G12S	CNA
ROS1	CNA	wt	wt	CNA	CNA	CNA
TP53	wt	Y220C	G262V	R273H; CNA	CNA	Deletion

From https://cellmodelpassports.sanger.ac.uk/ and https://depmap.org/portal/ ; wt: wild-type; CAN: Copy Number Alterations.

Supplementary Table 2. Clinical-pathological characteristics of NSCLC patients

Patient	Age	Sex	Histotype	Grading	Tumor size	Nodes	Smoking history	pre-ICB treatment	ICB	PD-L1 IHC	PD-L1 Score	Molecular Test	EGFR status	KRAS status	ALK status	ROS1 status	Other Mutations
IRE-PR04	69	F	ADC	G3	T2a	N0	No	chemo-tarceva	Nivolumab	nd	1	Real-Time	wt	nd	nd	nd	
IRE-PR05	54	F	ADC	G3	T4	N2	Yes	chemo	Nivolumab	nd	3	Real-Time	wt	nd	nd	nd	
IRE-PR06	71	M	SCC and SCLC	G2	T1b	N0	Ex smoker	chemo-RT	Nivolumab	nd	2	nd	nd	nd	nd	nd	
IRE-PR07	59	F	ADC	G3	T3	N1	Ex smoker	chemo	Pembrolizumab	50%	2	Oncomine ™ Solid Tumour	wt	G12D	nd	nd	
IRE-GR03	61	M	ADC	G3	T4	N3	Ex smoker	chemo	Nivolumab	nd	2	Oncomine ™ Solid Tumour	wt	wt	nd	nd	TP53 C176F
IRE-GR06	59	M	SCC	G2	T2a	N0	Yes	chemo-tarceva	Nivolumab	nd	2	nd	nd	nd	nd	nd	
IRE-GR07	57	M	ADC	G3	T3	N2	Yes	RT-chemo	Nivolumab	nd	1	Oncomine ™ Solid Tumour	wt	wt	nd	nd	
IRE-GR08	70	F	ADC	G3	T2a	N0	Yes	chemo-tarceva	Pembrolizumab	10%	2	Oncomine ™ Focus Assay	wt	wt	nd	nd	
IRE-GR09	60	M	SCC	G3	T3	N0	Ex smoker	chemo-RT	Pembrolizumab	60%	3	nd	nd	nd	nd	nd	
IRE-GR10	66	M	ADC	G3	T2a	N1	nd	chemo	Pembrolizumab	60%	3	Oncomine ™ Focus Assay	wt	wt	nd	nd	
HUM-GR05	43	F	ADC	G2	T1b	N0	No	chemo	Nivolumab	POS	1	nd	wt	nd	NEG	NEG	
HUM-GR10	74	M	SCC	G2	T2	N0	Ex smoker	chemo	Nivolumab	nd	1	nd	nd	nd	nd	nd	
HSR-PR06	60	M	ADC (Lynphonode mets)	nd	nd	nd	Ex Smoker	chemo	Nivolumab	nd	3	Sequenom	wt	wt	nd	nd	
HSR-PR07	57	F	ADC (Pleural mets)	nd	nd	nd	Yes	chemo-alimta	Nivolumab	0%	1	Sequenom	wt	nd	nd	nd	
HSR-PR10	67	M	ADC (Lung mets)	nd	nd	nd	Ex smoker	chemo-RT	Nivolumab	0%	3	Sequenom	wt	wt	nd	nd	

IRE: Regina Elena National Cancer Institute; HUM: Humanitas Research Hospital; HSR: San Raffaele Hospital; GR: good responder; PR: poor responder (as defined in Mat and Met); ADC: Adenocarcinoma; SCC: Squamous cell carcinoma; SCLC: Small Cell Lung Cancer; met: metastasis; RT: Radiotherapy; nd: Not determined; wt: wild type. PD-L1 Score based on Nanostring normalized counts.